UC San Diego
UC San Diego Previously Published Works

Title

Axonal amyloid precursor protein and its fragments undergo somatodendritic endocytosis and processing

Permalink

https://escholarship.org/uc/item/1jm0923r

Journal

Molecular Biology of the Cell, 26(2)

ISSN

1059-1524

Authors

Niederst, Emily D
Reyna, Sol M
Goldstein, Lawrence SB

Publication Date

2015-01-15

DOI

10.1091/mbc.e14-06-1049

Peer reviewed

eScholarship.org Powered by the California Digital Library
University of California

Axonal amyloid precursor protein and its fragments undergo somatodendritic endocytosis and processing

Emily D. Niederst*, Sol M. Reyna, and Lawrence S. B. Goldstein
Department of Cellular and Molecular Medicine, University of California, San Diego, La Jolla, CA 92093

ABSTRACT Deposition of potentially neurotoxic Aβ fragments derived from amyloid precursor protein (APP) at synapses may be a key contributor to Alzheimer's disease. However, the location(s) of proteolytic processing and subsequent secretion of APP fragments from highly compartmentalized, euploid neurons that express APP and processing enzymes at normal levels is not well understood. To probe the behavior of endogenous APP, particularly in human neurons, we developed a system using neurons differentiated from human embryonic stem cells, cultured in microfluidic devices, to enable direct biochemical measurements from axons. Using human or mouse neurons in these devices, we measured levels of Aβ, sAPPα, and sAPPβ secreted solely from axons. We found that a majority of the fragments secreted from axons were processed in the soma, and many were dependent on somatic endocytosis for axonal secretion. We also observed that APP and the β-site APP cleaving enzyme were, for the most part, not dependent on endocytosis for axonal entry. These data establish that axonal entry and secretion of APP and its proteolytic processing products traverse different pathways in the somatodendritic compartment before axonal entry.

Monitoring Editor
Paul Forscher
Yale University

Received: Jun 9, 2014
Revised: Sep 18, 2014
Accepted: Nov 5, 2014

INTRODUCTION

Alterations of expression or processing of amyloid precursor protein (APP) are pathogenic (Bertram *et al.*, 2010) and may lead to the characteristic synapse loss and neuronal death, which are key features of Alzheimer's disease (AD; Coleman and Yao, 2003; Wei *et al.*, 2009).

Despite extensive research into the mechanisms controlling proteolytic cleavage of APP, the subcellular location of processing and the relationship of proteolytic processing to sorting pathways in neurons remains unclear. Full-length APP undergoes multiple proteolytic processing events, typically an α- or β-site cleavage step followed by γ-site cleavage by secretase proteins (Haass *et al.*, 2012). Sorting of APP and its proteolytic fragments in bona fide neurons is less understood, with evidence for multiple pathways, including dendritic to axon sorting and axon transport preceding dendritic sorting (Simons *et al.*, 1995; Yamazaki *et al.*, 1995; Koo *et al.*, 1996). In addition, APP and the secretase β-site APP-cleaving enzyme (BACE), which mediates amyloidogenic β-site cleavage events, are internalized through endocytosis via different endocytic pathways (Schneider *et al.*, 2008; Sannerud *et al.*, 2011; Morel *et al.*, 2013). Importantly, and in contrast to nonpolarized cells, neurons have sophisticated sorting systems most similar to the pathways found in polarized epithelia. These pathways may also be altered substantially when APP and the secretases are overexpressed during typical experimental protocols.

Current evidence does not distinguish among multiple models for the location of APP processing in neurons and the sorting of full-length APP (FL-APP) and its fragments into axons. One model postulates that most APP is processed in the cell body and APP cleavage products are sorted into independent vesicles before entering the axon (Muresan *et al.*, 2009). This model is also supported by the

---

This article was published online ahead of print in MBoC in Press (http://www.molbiolcell.org/cgi/doi/10.1091/mbc.E14-06-1049) on November 12, 2014.

*Present address: Department of Neurobiology, Boston Children's Hospital, Harvard Medical School, Boston, MA 02115.

Address correspondence to: Lawrence S. B. Goldstein (lgoldstein@ucsd.edu).

Abbreviations used: βIIItub, β-III tubulin; AD, Alzheimer's disease; ANCOVA, analysis of covariance; ANOVA, analysis of variance; APP, amyloid precursor protein; BACE, β-site APP-cleaving enzyme; DAPI, 4′,6-diamidino-2-phenylindole; DMSO, dimethyl sulfoxide; FAD, familial AD; FITC, fluorescein isothiocyanate; FL-APP, full-length APP; hESC, human embryonic stem cell; PBS, phosphate-buffered saline; pen/strep, penicillin/streptomycin; p-NFH, phospho-neurofilament heavy chain; YFP, yellow fluorescent protein.

© 2015 Niederst *et al.* This article is distributed by The American Society for Cell Biology under license from the author(s). Two months after publication it is available to the public under an Attribution–Noncommercial–Share Alike 3.0 Unported Creative Commons License (http://creativecommons.org/licenses/by-nc-sa/3.0).
"ASCB®," "The American Society for Cell Biology®," and "Molecular Biology of the Cell®" are registered trademarks of The American Society for Cell Biology.

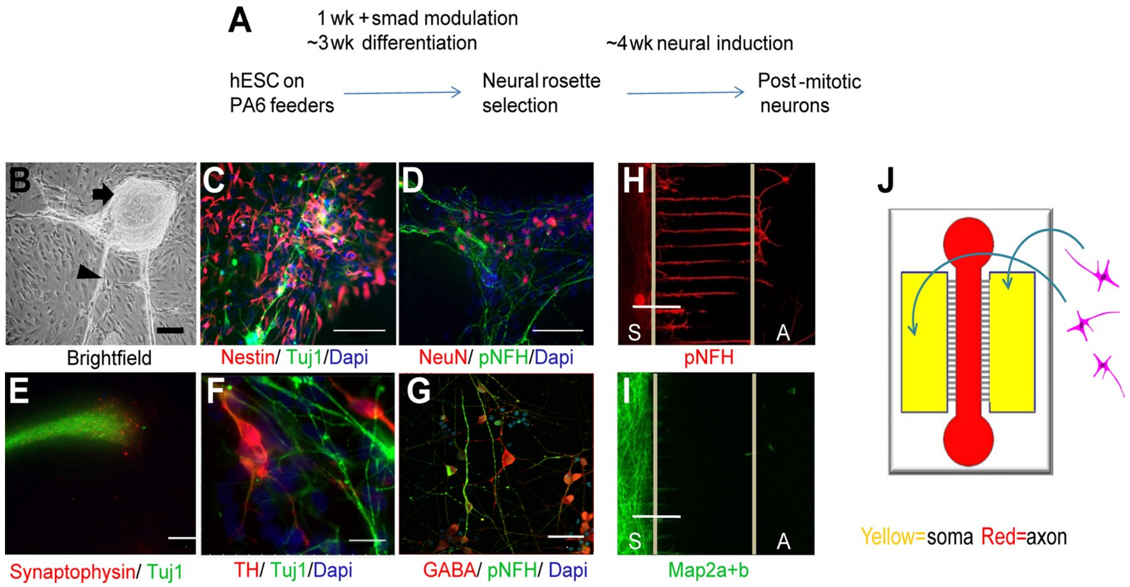

FIGURE 1: Human neuronal differentiation and microfluidic devices to fluidically isolate axons. (A) Schematic of differentiation steps. (B) Neural rosette (arrow) with neuronal projections (arrowhead) growing on PA6 feeder layers. (C) βIIItub (Tuj1) in green and nestin in red. (D) p-NFH axons in green and NeuN nuclei in red. (E) Synaptophysin in red and Tuj1 in green. (F) Tyrosine hydroxylase in red and Tuj1 in green. (G) GABA in red and p-NFH in green. Scale bars: (B–D and G) 100 µm; (E) 10 µm; (F) 20 µm. (H and I) p-NFH (in red) and Map2 (in green) immunofluorescence of human day 36 neurons in microfluidic chambers. White lines denote fluidic barriers; S, soma; A, axons. (J) Diagram of new microfluidic chamber design. Neurons are plated in the two somal chambers (yellow), and one central axonal chamber is shown in red.

finding that the endocytic sorting pathway for the β-secretase is limited largely to the soma, where processing is postulated to occur (Sannerud *et al.*, 2011).

Another model proposes local processing in axons/synapses, with extracellular APP fragments potentially secreted directly from the region in which they were processed. This model is supported by evidence for colocalization of processing enzymes together with APP in vesicles (Kamal *et al.*, 2001) and evidence that synaptic activity in vivo increases endocytosis-dependent Aβ release into the brain (Cirrito *et al.*, 2008; Tampellini *et al.*, 2009; Das *et al.*, 2013). The finding that Aβ secretion can depend on both synaptic activity and endocytosis implicates the synapse as a site of processing and secretion.

It is feasible that some combination of these two pathways occurs in neurons; however, the subcellular sorting and processing of endogenous APP in neurons has not yet been directly examined. The location of Aβ and its accompanying toxicity, be it synaptic or diffuse, axonal or dendritic, is dependent on the location of secretion and processing of APP in neurons. Additionally, shifts in the location of Aβ secretion may be part of the disease process. Thus discovering the subcellular details of APP processing and secretion is important for insight into the AD process.

To understand typical APP sorting and processing, it is important to study pathways and processing in the context of endogenous levels of APP protein. This is because there is considerable evidence that overexpression of APP can alter the sorting and trafficking of APP in neurons (Cataldo *et al.*, 2003; Muresan and Muresan, 2007). In fact, overexpression of APP can cause alterations in axonal transport dynamics and change the content of axonal APP vesicles (Torroja *et al.*, 1999; Gunawardena and Goldstein, 2001; Stokin *et al.*, 2005; Muresan *et al.*, 2009). Furthermore, a single extra copy of APP in the human genome will cause early-onset AD (Lai and Williams, 1989; Sleegers *et al.*, 2006). However, research on endogenous APP in neurons has been limited due to several technical constraints.

To better understand endogenous APP processing, localization, secretion, and sorting of APP and its fragments in neurons, we took advantage of compartmentalized culture systems that enable biochemical analyses by separating axons from bulk neuronal cultures (Taylor *et al.*, 2005; Park *et al.*, 2009). To test whether the details of APP processing are conserved between mice and humans, we also developed a compartmentalized system suitable for human neurons.

We determined, in mouse and human neurons, that a significant majority of endogenous APP proteolytic fragments secreted from axons were processed in the neuronal soma. Additionally, we found that APP proteolytic fragments secreted from axons were generated in a pathway that depends upon somatic endocytosis. In contrast, full-length unprocessed APP and BACE appeared to be sorted into axons through at least two pathways, one dependent on endocytosis, one not. These results suggest that sorting and processing of APP in neurons is more complex and highly regulated than previously thought and involves a minimum of two separable pathways.

RESULTS

Human neurons differentiated from embryonic stem cells

To obtain human neurons in sufficient quantities for biochemical measurements, we developed a method to differentiate neurons from human embryonic stem cells (hESCs). This protocol produces postmitotic neurons expressing endogenous amounts of human proteins. The timeline and procedure is briefly outlined in Figure 1A and is a combination of previously published protocols (Chambers *et al.*, 2009; Yuan *et al.*, 2011). Specifically, hESCs were seeded onto PA6 feeder cells, cultured 1 wk in the presence of SMAD inhibitor and noggin, and then cultured an additional 3 wk for neuronal precursor induction. Neural rosettes (Figure 1B) were selected, and cells were cultured another ~4 wk with BDNF, GDNF, and cAMP for neuronal differentiation.

Following differentiation, cells expressed several postmitotic neuronal markers such as β- III tubulin (βIIItub; Figure 1C), the neuronal nuclei marker NeuN (Figure 1D), polarity markers phosphoneurofilament heavy chain (p-NFH; axonal; Figure 1, D and H) and Map2 a+b (dendritic; Figure 1I), as well as synaptic proteins such as synaptophysin (Figure 1E) and neurotransmitter markers such as TH (Figure 1F) and GABA (Figure 1G). Efficiency of neuronal induction varies between hESC lines, but the addition of SMAD inhibitors and noggin reduces this variation. The efficiency and neurotransmitter type are described in previously published reports for this PA6-based induction method (Buytaert-Hoefen *et al*., 2004; Israel *et al*., 2012). The successful and consistent differentiation of hESCs into neurons via stromal induction allowed for biochemical or other analysis of endogenous human neuronal proteins.

Fluidic separation of axons from neuronal cell bodies

Region-specific aggregation of Aβ and synaptic toxicity of APP fragments raised the possibility that the regional processing and secretion of APP within a neuron may be an important factor in the pathogenesis of AD (Brunholz *et al*., 2012). To directly determine the subcellular location of processing and secretion of endogenous APP fragments from neurons, we developed a microfluidic culture system to separate axons from bulk neuronal culture. Microfluidic culture systems can isolate pure axons without contamination from cell soma or dendrites (Taylor *et al*., 2005). The chamber design used in past publications did not provide enough cellular material to do biochemistry and were designed for dissociated cells.

Thus we developed a modified design that would both maximize the number of pure axons for biochemical analysis, as well as allow for culture of human rosettes during differentiation, which can be cell masses several millimeters in diameter. Our design entails two open "soma" compartments (3 mm × 23 mm × 10 mm) connected by capillary channels to a single central "axonal" channel compartment (3 mm × 100 μm × 39 mm) (Figure 1J). The connecting capillary channels (10 μm × 3 μm × 450 μm) draw axons from human or mouse neurons to project through to the axon compartment but are sufficiently long to exclude dendrites. Fluidic isolation of compartments was established by adding a slightly higher medium volume in the axonal compartment, thus creating a slow flow into the somal compartment, which prevents diffusion of somal contaminants into axonal samples. This hydrostatic differential ensures that materials secreted from axons can be selectively and rigorously evaluated.

We discovered that there was a significant failure rate of fluidic isolation in these and other previously described types of compartments due to leakage of chambers. Thus we found it essential to verify fluidic isolation in our experiments by routinely testing isolation of the axonal compartment using a 4-kDa fluorescein isothiocyanate (FITC)-labeled dextran. FITC-dextran was not detectable in the axonal chamber after 24 h (Supplemental Figure S1A). In all subsequent microfluidic chamber experiments, labeled dextran was always included in the somal media to detect and exclude the ~5% of chambers that leak somal compartment components into axonal compartments.

Neurons differentiated from hESCs extended p-NFH–positive (Figure 1H and Supplemental Figure S1B) axons into the axonal chamber, while Map2-positive dendrites were excluded (Figure 1I). Primary neuronal cultures from wild-type mouse hippocampi also grew well in modified culture chambers and, after 10 d in vitro, sent robust, βIIItub-positive axonal projections through the channels, while Map2-positive dendrites were excluded (Supplemental Figure S1, C and D).

Axons of neurons expressing endogenous APP secrete sAPP and Aβ

To directly measure the secretion of APP fragments from axons versus bulk somal culture (composed of soma/dendrites and axons), we cultured primary hippocampal neurons for 10 d in microfluidic chambers and then applied fresh media to both somal and axonal compartments. An additional volume of 50 μl in the axonal compartment maintained fluidic isolation of the axons. After 24 h, conditioned media were collected and Aβ amounts were measured by electro-chemiluminescent (ECL) immunoassay, which is sufficiently sensitive to detect endogenous APP fragments secreted from the ~2000 axons present in a chamber (see *Materials and Methods*). No assay was found to reliably detect mouse sAPPα at these concentrations. The immunoassay used the 4G8 antibody to detect mouse Aβ, which could also, in theory, detect P3. Specificity of the 4G8 kit was tested with human conditioned media on both the 4G8 kit and a 6E10 human-specific kit, which does not detect P3. No difference in Aβ measurements was detected between the two kits, indicating that 4G8 measurements of Aβ are not significantly affected by P3 levels.

Axons from mouse hippocampal cultures were found to secrete detectable amounts of Aβ40, whereas Aβ38, Aβ42, and sAPPβ were below detection limits in these experiments. The concentration of Aβ40 in the axonal compartment after 24 h of axonal secretion averaged 17.1 ± 4.9 pM per chamber, while the bulk culture (whole neurons) contained an average of 588 ± 364 pM of Aβ40 after 24 h of somatic secretion ($n = 13$; Figure 2A). The number of molecules secreted from an individual axon was determined by fixation of a subset of chambers and counting of p-NFH–positive axons (mean 1030 ± 130 axons/chamber). Previous work measuring Aβ in brain slices or cultures with established synapses indicates a majority of Aβ is released through synaptic vesicle exocytosis and is therefore most likely secreted solely from axon terminals (Cirrito *et al*., 2008; Tampellini *et al*., 2009). As such, we treated each axon as a point source for Aβ secretion. Additionally, axonal staining compared with Aβ measurements showed concentrations of Aβ were independent of whether axons had just begun to enter the axon compartment or were fully extended. The Pearson's correlation coefficient between Aβ40 concentrations and axon number is 0.78 for mouse and 0.87 for human samples. We calculated the amount of secretion per axon by multiplying the sample volume (150 μl in the axonal compartment and 125 μl in each somatic chamber) by the APP fragment concentration, divided by the number of axons per chamber. To estimate the number of molecules secreted, we multiplied the fragment concentration by Avogadro's number, which results in an estimate of $4.0 \times 10^5 \pm 6 \times 10^4$ Aβ40 molecules secreted per axon over a 24-h period (Figure 2B). This may be an underestimate of total Aβ secretion, as some protein may be degraded over the 24-h sampling period.

For calculation of the number of molecules secreted per soma, cell number was quantified by counting NeuN-positive nuclei (~60,000 nuclei per chamber). As only ~2% of the neurons in a chamber are near enough to the microfluidic channels to project axons through, 98% of the cells in the somal compartment also have axons in that compartment. To account for the axonal contribution of Aβ to the somal measurements, we estimated the axonal number by subtracting the number of axons in the axonal compartment from the number of cells in the somal compartment. This assumes that each cell has one axon and that axons in the axonal compartment secrete the same amount as axons in the somal compartment. The axonal contribution was calculated by multiplying the number of molecules per axon by the number of axons in the somal compartment and

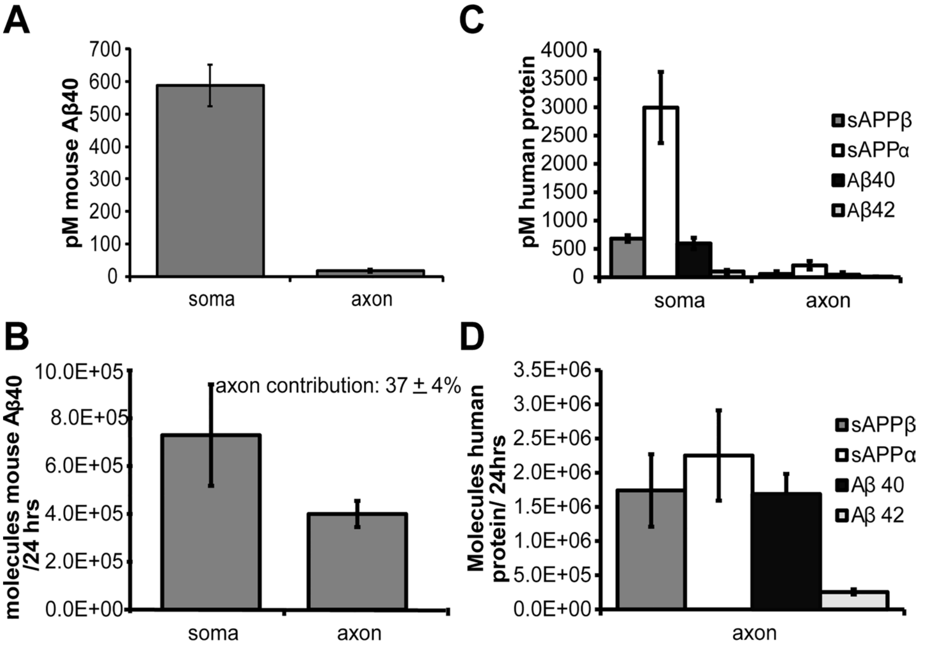

FIGURE 2: Mouse and human neurons secrete APP fragments from axons. (A) Secreted Aβ40 from mouse hippocampal neurons after 24 h. (B) Number of molecules of Aβ40 secreted per axon or cell body of mouse neurons in 24 h. (C) sAPPβ, sAPPα, and Aβ40 and Aβ42 measurements from human differentiated neurons after 24 h, in compartments 30–40 d. (D) Number of molecules of sAPPβ, sAPPα, and Aβ40 and Aβ42 secreted per axon of human neurons in 24 h. Error bars are SE.

was subtracted from the somal compartment totals. Aβ amounts were then calculated as noted above. This calculation yields an estimate of $7.3 \times 10^5 \pm 2 \times 10^5$ molecules of Aβ40 secreted per soma (Figure 2B).

From these measurements, we can thus calculate that an average of 37 ± 4% of total neuronal Aβ40 is secreted from the axons, per neuron, from mouse hippocampal neurons (calculated by dividing the number of Aβ40 molecules secreted by axons to that secreted by the sum of Aβ40 secreted by axons and soma for each compartment). Our data provide the first direct, quantitative measurement of endogenous Aβ secretion from any type of axon.

Human neurons differentiated from hESCs were cultured in compartments and also sampled for APP fragment secretion in analogous experiments. Axons were fluidically isolated, and media were collected 24 h later. Axons from human neurons secreted detectable amounts of Aβ40, Aβ42, sAPPβ, and sAPPα. Axonal conditioned media from human neurons contained 45 ± 10 pM Aβ40 and 10 ± 3 pM Aβ42 in 200 µl media per chamber, and bulk (soma) culture conditioned media contained 600 ± 100 pM Aβ40 and 100 ± 30 pM Aβ42 in 200 µl of media over 24 h ($n = 14$; Figure 2B). This is approximately a 5:1 ratio of Aβ40:42 in the axonal compartment and 6:1 ratio in the somal compartments, which is similar to published human brain samples (Lewczuk *et al.*, 2004). Additionally, sAPPβ was measured in media at a concentration of 58 ± 10 pM in the axon and 680 ± 60 pM in the bulk (soma + axon) neuronal compartment, while sAPPα was measured at 210 ± 80 pM in the axon compartment and 3000 ± 630 pM in the somal compartment ($n = 14$; Figure 2C). Soluble APP fragments showed higher variability than other measurements, possibly due to degradation or cleavage after secretion.

The neuronal rosettes used for differentiation of human neurons produce large masses of neurons. Owing to these aggregates and the presence of nonneuronal cells, it was not possible to get per-soma measurements similar to the mouse measurements. However, for a subset of chambers, per-axon measurements were obtained using the same calculations as used for the hippocampal neurons. These calculations revealed that $1.7 \times 10^6 \pm 5.3 \times 10^5$ molecules of sAPPβ, $2.3 \times 10^6 \pm 6.6 \times 10^5$ molecules of sAPPα, $1.7 \times 10^6 \pm 3.0 \times 10^5$ molecules of Aβ40, and $2.6 \times 10^5 \pm 1.1 \times 10^4$ molecules of Aβ42 were secreted per axon over a 24-h period ($n = 7$; Figure 2D). Chambers containing human neurons averaged 1600 ± 110 axons each. Thus axonal secretion of Aβ40 was ~4 times higher from human neurons than from mouse neurons, possibly due to neuronal type or species differences. Also worth noting, the sAPPβ to Aβ ratio is 1:1, the expected ratio if γ cleavage is near complete on β-cleaved C-terminal fragments.

Most APP fragments secreted from axons are processed in the cell soma

Previous work has led to multiple models for the location and sorting of endogenous APP into axons. One potential model proposes that APP processing occurs mainly in the soma, while another model proposes that most APP is processed locally in the axon shafts and/or synapses. An additional, intermediate possibility is that neurons process APP both in the soma and the axon and can alter the location of processing depending on signaling, neuronal cell type, or other local conditions.

To distinguish among the possible models and to determine the location of APP processing in neurons, we again utilized microfluidic chambers. In addition to allowing for isolation of axons, the chambers permit localized drug treatment of somal compartments. To determine the location of processing of APP in mouse and human cultured neurons, we applied inhibitors of the APP-processing proteases (secretase inhibitors) to the cell soma while the axons were kept in isolation.

In hippocampal cultures, we found that inhibition of soma β- or γ-secretase activity caused a significant decrease in secretion of Aβ40 from the axons compared with vehicle-treated controls (Figure 3A). Inhibition of β-secretase in the somal compartment by the inhibitor OM99-2 at 1 µM (β-inh) for 24 h reduced somal Aβ40 to 43 ± 5% (one-way analysis of variance [ANOVA]: $p < 0.0001$; Tukey post hoc: $p < 0.05$; $n = 6$), with a trend toward reduction in axonal Aβ40 to 64 ± 30% (n.s.; $n = 6$; Figure 3A). Inhibition of somal processing using 200 nM Compound E, a γ-secretase inhibitor, for 24 h reduced somal compartment Aβ40 secretion to 12% ± 2% of vehicle (Tukey post hoc: $p < 0.0001$; $n = 12$). Concurrent secretion of Aβ40 from axons was reduced to 30% ± 10% of vehicle (one-way ANOVA: $p < 0.05$; Tukey post hoc: $p < 0.05$; $n = 12$; Figure 3A). Finally, inhibition of both somal and axonal compartments resulted in a decrease of somatic Aβ40 to 9% ± 2% of vehicle (Tukey post hoc: $p < 0.001$; $n = 5$) and a concurrent decrease in axonal Aβ to 26% ± 9% of vehicle. Secreted Aβ was normalized to the number of βIIItub-positive axons extending 40 µm into the axon compartment (to distinguish individual axons) and to the average number of nuclei for samples from the somal compartment. As the axonal Aβ was reduced only 18 ± 10% less than the directly inhibited soma, we conclude that

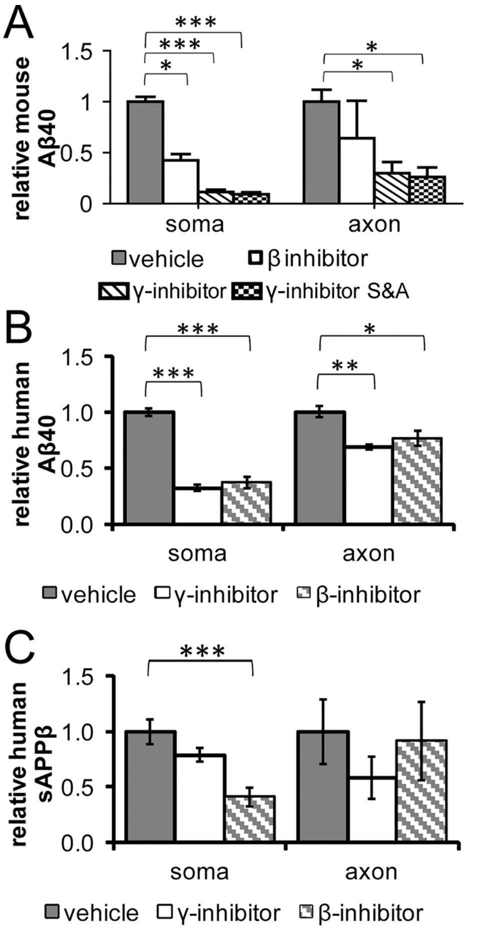

FIGURE 3: Inhibition of secretase activity in soma reduces axonal secretion of Aβ. (A) Aβ40 from mouse hippocampal neurons in compartments, relative to vehicle control. Samples were treated with vehicle (DMSO), β inhibitor (OM99-2), or γ inhibitor (Compound E) in the somal compartment, or γ inhibitor on soma and axon (S&A) for 24 h before collection. (B) Aβ40 from human neurons in compartments, treated with vehicle, γ inhibitor (Compound E), or β inhibitor IV for 24 h in the somal compartment, relative to control. (C) sAPPβ from human neurons in compartments, treated with vehicle, γ inhibitor (Compound E), or β inhibitor IV on the soma for 24 h, relative to control. Error bars are SE; *, $p < 0.05$; **, $p < 0.01$; ***, $p < 0.001$.

70–90% of γ processing occurred in the soma. The difference in axonal secretion between soma-only γ inhibition (to 30%) and total (somal and axonal) inhibition (26%) was only 4%, indicating that up to 96% of axonal Aβ produced in this time frame could be processed in the soma. The lack of inhibition of axonal Aβ to levels seen in the somal samples, even with global application of inhibitor, may represent a pool of intracellular axonal Aβ that can be released over time, even during secretase inhibition. For β processing, axonal Aβ was 22 ± 30% less reduced than directly inhibited soma, so 40–100% of β processing occurred in the soma. The high variance of axonal Aβ resulted in the large range estimates. However, the general trends toward somatic processing and axonal secretion are striking, despite biological variance. Overall our measurements suggest that 70–90% of Aβ secreted from axons was processed in the soma in hippocampal neurons in these conditions.

A similar result was also obtained in human differentiated neurons. Neurons in compartments were treated with somal application of secretase inhibitors as in the mouse experiments. In human cells, Aβ40 secretion was reduced in the soma by 200 nM Compound E to 32 ± 4% of vehicle (one-way ANOVA: $p < 0.0001$; Tukey post hoc $p = 0.0001$; $n = 5$), and in the axons to 68 ± 3% of vehicle (one-way ANOVA: $p < 0.001$; Tukey post hoc: $p = 0.001$; $n = 4$) (Figure 3B). Additionally, β inhibitor IV reduced somal Aβ to 37 ± 5% ($p = 0.0001$; $n = 5$) and axonal Aβ to 77 ± 7% ($p = 0.008$; $n = 4$). sAPPβ was reduced in soma to 41 ± 8% of vehicle (one-way ANOVA: $p < 0.001$; Tukey post hoc: $p = 0.0002$) by β inhibitor but not significantly changed by Compound E (decreased to 79 ± 6%; $p = 0.07$) (Figure 3C). Axonal measurements of sAPPβ varied widely and thus showed no significant differences (one-way ANOVA: $p = 0.41$). These results could indicate sAPPβ itself is not transcytosed, or they may reflect the high variance in this experiment masking possible drug effects. In human neurons, 50–70% of Aβ secreted from axons was β cleaved in the soma, and 60–70% was γ cleaved in the soma. Direct inhibition of axonal processing is not possible, due to the flow of media from the axon compartment into the somal compartment during axonal isolation, leading to inhibition of both compartments.

It is interesting to note that, although human neurons show consistent reduction of axonal Aβ secretion upon somatic inhibition of processing, this reduction is smaller in magnitude than in the mouse hippocampal cultures (60–70% in human vs. 70–90% in mouse hippocampal neurons). The increase in local axonal processing may represent differences between species or neuron type and further underscores the importance of studies on human neurons.

To address the possibility that inhibitor applied in the somatodendritic compartment may be bound and actively transported into axons, effectively inhibiting processing locally in axons, we calculated the possible contribution of drugs applied to the soma that could affect axonal processing. With a maximum axon diameter of 0.8 μm, an axon length of 1 mm, and an average of 1600 axons per chamber, the total axonal volume would be ~8×10^{-4} mm^3. With an axonal compartment volume of 200 μl of media, we calculated the volume of axons in the axonal chamber to be 1/250,000th the volume of media in the axonal chamber. The inhibitors are not preferentially retained within the cell, so this dilution would lead all inhibitors to diffuse away from the enzymes into the untreated axonal media. This dilution factor leads to a maximum possible drug concentration of 0.8 pM for Compound E, 4 pM for OM99-2, and 8 pM for β inhibitor IV, which is well below the inhibitory constants of the inhibitors (IC$_{50}$ = 100 nM Compound E, IC$_{50}$ = 70 nM OM99-2, IC$_{50}$ = 36 nM β inhibitor IV; Seiffert *et al.*, 2000; Stachel *et al.*, 2004; Garino *et al.*, 2006). Therefore these estimates suggest that the effect on axonal secretion is not caused by local inhibition due to inhibitor transported from soma to axon.

Somatic processing of many axonal APP fragments requires endocytosis

If APP fragments are generated in the soma before transport into axons, it is important to determine the pathways of APP processing and sorting before axonal entry. One possibility is that processing of APP occurs in the Golgi/secretory pathway en route to sorting of secretory-derived vesicles into the axon. However, it has been reported that BACE activity is enriched in late or recycling endosomes and that endocytosis is required for the production of a significant portion of the Aβ secreted from nonneuronal and neuronal cells (Koo and Squazzo, 1994; Kinoshita *et al.*, 2003; Carey *et al.*, 2005).

We tested whether APP fragments and/or the secretase machinery are endocytosed from the somatodendritic cell membrane before being sorted into axons. This pathway has been suggested for various axonal proteins, including L1/NgCAM, TrkA, Caspr2, and CB$_1$R (Wisco *et al.*, 2003; Leterrier *et al.*, 2006; Ascano *et al.*, 2009;

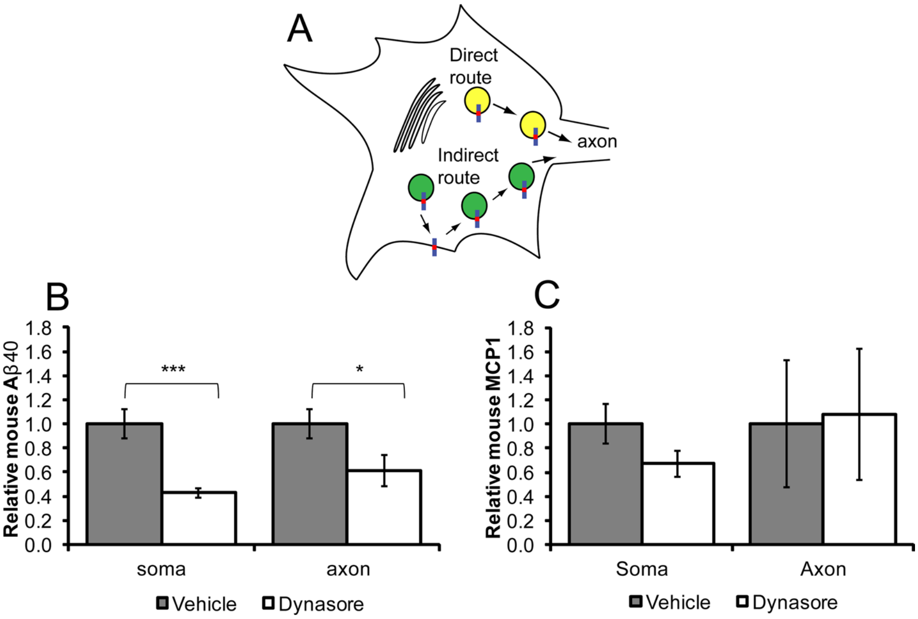

FIGURE 4: Inhibition of somatic endocytosis reduces axonally secreted Aβ. (A) Neuronal transcytosis. Yellow vesicles are proposed to travel by a direct, secretory pathway, while the green vesicles travel via an indirect, endosomal transcytosis pathway. (B) Somal compartments treated with vehicle (DMSO) or dynasore. Mouse Aβ40 from hippocampal neurons normalized to nuclei or axon number, relative to vehicle control. (C) Mouse MCP1 from same samples as in B, normalized to nuclei or axon number, relative to control. Error bars are SE; *, $p < 0.05$; ***, $p < 0.001$.

Bel *et al.*, 2009). This endocytosis and sorting pathway is termed "transcytosis" and is comparable with the sorting process from basolateral to apical membranes that occurs in polarized epithelia (Figure 4A).

To test the hypothesis that axonal APP fragments are dependent on somatic endocytosis, we first evaluated whether Aβ secretion from axons was dependent on endocytosis in the cell body. To do this, we used the dynamin inhibitor dynasore (Macia *et al.*, 2006). Dynasore effectively inhibited clathrin-mediated endocytosis in hippocampal neurons, as demonstrated by uptake of Alexa Fluor 568–transferrin, the internalization of which was robust in neurons and was 95% inhibited by 100 μM dynasore after 4–6 h (unpublished data) and 60% inhibited after 24 h of treatment (Supplemental Figure S2, A and B). We applied dynasore to hippocampal neurons in chambers, such that dynasore was applied to somal compartment medium while the axonal compartment was isolated. After 24 h, medium was collected and sampled for Aβ40. The Aβ40 secreted from hippocampal neurons in the somal compartment after dynasore treatment was reduced to 43 ± 4% of vehicle (*t* test: $p = 5 \times 10^8$) compared with vehicle-treated controls (Figure 4B), similar to previously published results of endocytic inhibition (Carey *et al.*, 2005). As can be seen in the transferrin uptake assay (Supplemental Figure S2B), inhibition by dynasore after 24 h was incomplete, so some Aβ was still produced. Axonal Aβ40 was also reduced to 61 ± 10% ($p = 0.013$) upon somal treatment with dynasore (Figure 4B). The difference between the reduction in the directly inhibited soma and uninhibited axons was 18 ± 10%. This suggests that 70–90% of inhibitable axonal Aβ was dependent on endocytosis in the soma, comparable with the percentages of axonal Aβ that were processed in the soma in the secretase experiments.

To confirm that transcytosis was not due to a global disruption of axonal sorting caused by endocytic inhibition, we also measured axonal and somal secretion of MCP1. MCP1 is a chemokine secreted from axons and should not depend on endocytosis for production. MCP1 sorting has not been associated with APP in normal neurons. As predicted, axonal MCP1 secretion was not reduced by endocytosis inhibition (Figure 4C), indicating that the effect on axonal secretion of Aβ40 is not due to a global disruption in axonal sorting or cell toxicity. Together these data indicated that endocytosis in the soma is a major pathway for the generation of axonal Aβ.

FL-APP is not sorted into axons via transcytosis

The evidence that 70–90% of APP fragments secreted from axons required somatic endocytosis before axonal entry led us to ask whether APP itself was sorted into the axon following endocytosis from the somatodendritic cell membrane. Previous literature has been contradictory regarding the pathway utilized by APP for delivery to axons (Koo *et al.*, 1990; Simons *et al.*, 1995; Cai *et al.*, 2003).

To test whether FL-APP sorting into axons is endocytosis dependent, we used the endocytosis inhibitor dynasore on hippocampal neurons. Cells were labeled with an N- or C-terminal antibody to APP and the dendritic marker Map2 (Figure 5A). If fragments were sorted separately from each other, discordance between the N- and C-terminal antibodies would be expected. The specificity of the antibodies was verified in $APP^{-/-}$ mice. The immunofluorescence intensity of the C-terminal antibody was dramatically diminished in $APP^{-/-}$ neurons, with most of the vesicles barely in the detectable range (Supplemental Figure S3A). Thus this antibody is suitable for overall neurite intensity measurements. The N-terminal antibody (labeled APP A8967) also had no decrease in vesicle number but showed a modest decrease in vesicle intensity, indicative of moderate nonspecific staining (Supplemental Figure S3C). The specificity of these antibodies was taken into account when interpreting experiments.

The distribution of staining in whole dendrites versus axons (D:A ratio) was quantified. For proteins previously demonstrated to travel to axons via transcytosis, inhibition of endocytosis greatly reduced the appearance of the protein in axons and increased in dendrites (represented by an increase in D:A ratio; Yap *et al.*, 2008). In untreated neurons, APP levels were slightly higher in dendrites than in axons (N-terminal antibody D:A = 1.7 ± 0.1, C-terminal antibody D:A = 1.5 ± 0.1; Figure 5B). Although the N-terminal D:A ratio was slightly higher than with a C-terminal antibody, these ratios were not significantly different when tested by analysis of covariance (ANCOVA). Unlike proteins shown to be transcytosed, the D:A ratio of APP was unchanged after 24 h of dynasore treatment (N-terminal antibody D:A = 1.8 ± 0.07, C-terminal antibody D:A = 1.4 ± 0.05; Figure 5B). ANCOVA tests show the D:A ratios did not significantly change between conditions (change in slopes: N-terminal $p = 0.13$, C-terminal $p = 0.86$), and overall brightness values did not significantly change (change in intercepts: N-terminal $p = 0.65$, C-terminal $p = 0.64$). In contrast, a 6-h cycloheximide treatment decreased axonal APP staining 75%, and axonal intensity decreased 15% after 1 h of cycloheximide treatment (unpublished data), establishing the sensitivity of our assay to changes as small as 15%.

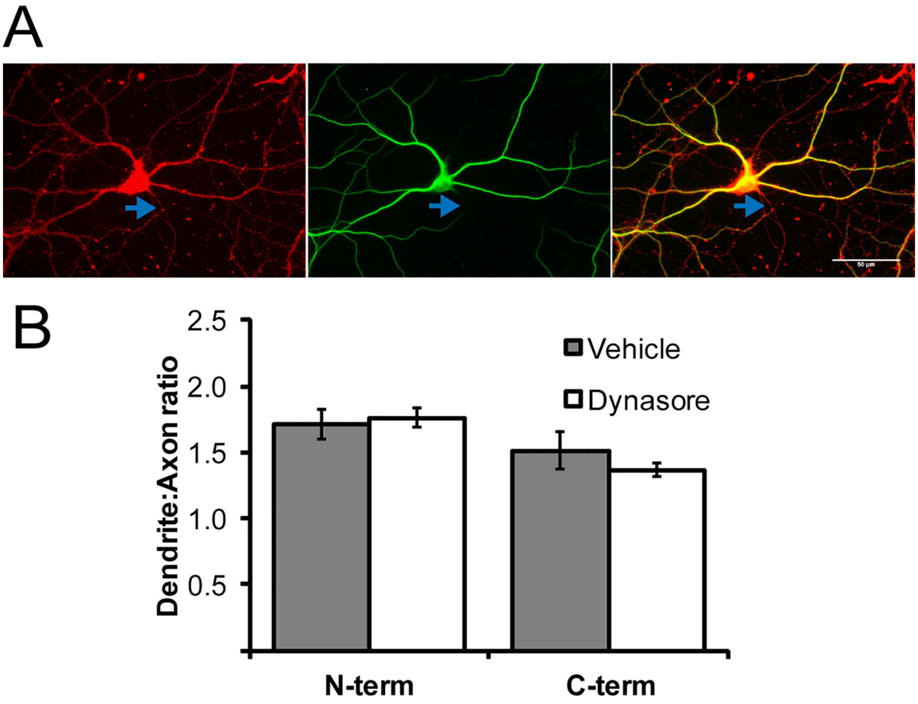

FIGURE 5: APP does not require somatic endocytosis for axonal delivery. (A) Immunocytochemistry of mouse hippocampal neuron. Green is Map2, labeling dendrites. Red is a C-terminal APP antibody. Blue arrow denotes a Map2-negative axon. Scale bar: 50 µm. (B) Quantification of neurons labeled as in A. APP N-terminal– (A8967) and C-terminal– (Chemicon) specific antibody-labeled neurons treated with vehicle or dynasore for 24 h. Dendrite to axonal fluorescence ratio is calculated. Error bars are SE.

Axonal APP fluorescence and D:A ratio were unchanged with either N- or C-terminal antibody, leading us to conclude that APP can enter the axons in an endocytosis-independent pathway, either during normal axonal sorting or specifically during endocytosis inhibition.

To address the possibility that axonal APP immunofluorescence is not affected by dynasore treatment due to a stabilized pool of APP that remained in the axons during the duration of dynasore treatment, or due to nonspecific binding of antibodies, we undertook another approach to test for transcytosis of FL-APP. In this assay, we measured FL-APP–yellow fluorescent protein (YFP) particle movement in axons proximal to the cell body (Supplemental Figure S4A). Neurons were pretreated for 4 h with dynasore and then imaged live to measure movement of APP-YFP vesicles. The number of anterograde-moving particles entering the axon from the cell bodies was not decreased by dynasore treatment (vehicle = 274 vesicles, dynasore = 218 vesicles; Supplemental Figure S4B). This confirms the observation that APP can enter the axon during endocytic inhibition.

Endosome-derived populations of APP vesicles in axons

Our results indicate that APP fragments undergo a complex sorting process before axonal entry. Multiple mechanisms can explain this phenomenon. One scenario includes FL-APP traveling through multiple pathways, both directly to the axon through the secretory pathway in an unprocessed form, as well as through transcytosis, where it would encounter the secretase machinery and be processed, and some or all fragments transported into axons. Another possibility is that FL-APP that is targeted to axons does not travel to the somatic cell surface but rather intersects in the soma with an intermediate, endosome-associated vesicle containing the processing machinery. This hybrid secretory/endocytic route has been observed in polarized epithelia for cargo such as p75 and apical-variant VSVG (Weisz and Rodriguez-Boulan, 2009). If FL-APP indeed arrives in the axons through multiple delivery pathways, APP vesicles would belong to various vesicle populations.

For determining the identity of axonal APP vesicles, differentiated human neurons were fixed and labeled by immunofluorescence for both APP and endosomal markers (Figure 6). High-resolution images of axons were acquired and analyzed using a Matlab software package described previously (Szpankowski *et al.*, 2012). This meticulously validated software uses a detection algorithm to determine subpixel locations of puncta by fitting Gaussian functions to the fluorescence data and is particularly well suited to rigorous and quantitative colocalization analysis when analyzing images densely populated with punctate vesicular staining.

The APP puncta (vesicles) were colocalized with Rab11 (recycling endosome; Figure 6A), Rab5 (early endosome; Figure 6B), or Rab7 (late endosome; Figure 6C) vesicles and BACE (Figure 6D). APP colocalization with endosome markers or BACE was not dependent on location within the axon, as shown in Figure 6, E and F.

Next we determined whether APP puncta populations in the axon changed after dynasore treatment. The effects of dynasore on APP in human neurons were confirmed, with an increase in antibody-labeled surface APP after dynasore treatment (Figure 7A); reduced levels of Aβ38, 40, and 42; and a slight increase in the sAPPα/β ratio (Supplemental Figure S5, A and B). APP undergoes α cleavage on the cell surface, so some of the FL-APP expected to accumulate at the surface is instead secreted as sAPPα.

APP puncta were labeled with two N-terminal or C-terminal antibodies to elucidate any possible sorting discrepancies between FL-APP or N- and C-terminal fragments and to control for antibody ambiguity. The Epitomics and APP "Jonas" C-terminal antibodies were used for C-terminal staining, as the Epitomics antibody has been previously characterized (Guo *et al.*, 2012), and the Jonas antibody showed both a decrease in vesicle intensity and number in APP knockout neurons (Supplemental Figure S3B). N-terminal antibodies were 5a3/1g7 (Koo and Squazzo, 1994) and a less-specific sigma N-terminal antibody A8967, characterized in Supplemental Figure S3C. All APP-positive puncta were detected and counted, and then double-labeled puncta were detected and measured as a percentage of total APP vesicles. Puncta density, percent colocalization, and staining intensity (vesicle loading) were measured in axons of vehicle- and dynasore-treated neurons.

Measurements of puncta density were calculated as puncta detected per micrometer. A slight but significant reduction in APP C-terminal puncta density was observed after 18 h of endocytic inhibition (APP Epitomics: 89 ± 3%, $p = 0.003$, vehicle $n = 43$ axons, dynasore $n = 39$ axons; APP Jonas: 92 ± 2%, $p = 0.0004$, vehicle $n = 37$, dynasore $n = 44$; Figure 7B). A slight increase in N-terminal vesicle density was observed with APP N-terminal antibody A8967 (108 ± 4%, $p = 0.03$) but was not confirmed with antibody 5a3/1g7.

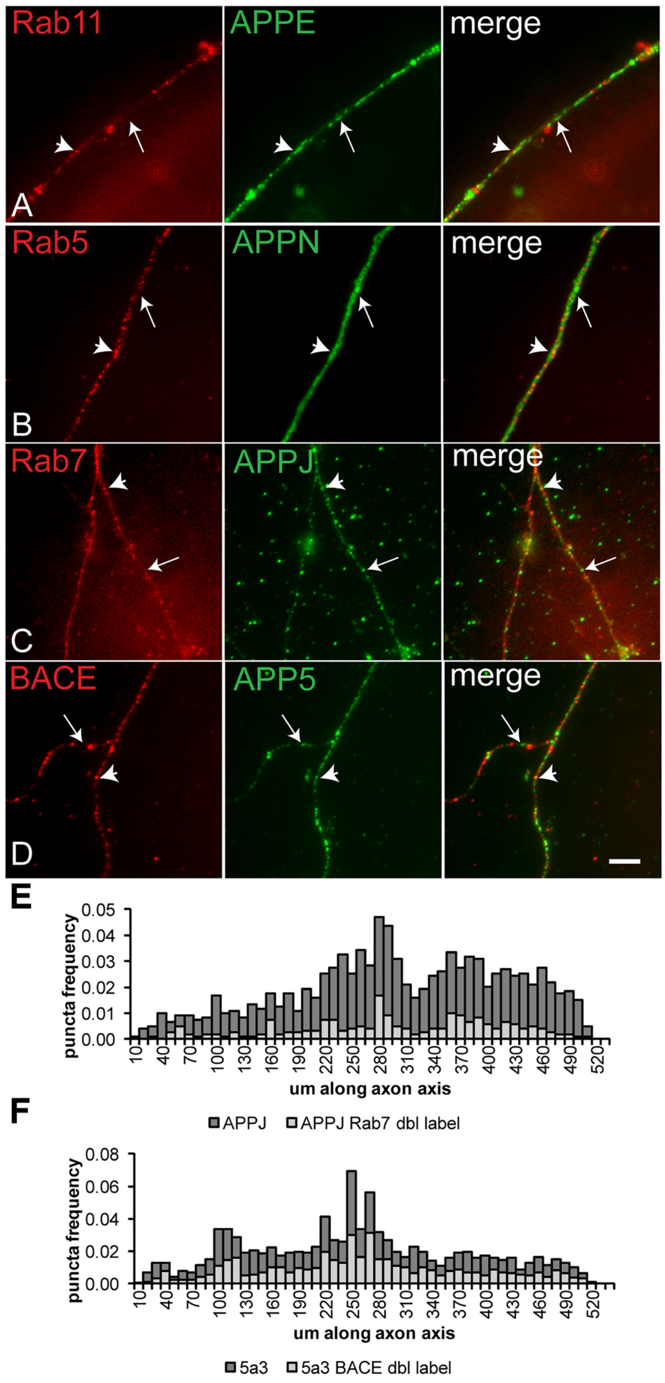

FIGURE 6: Axonal APP vesicles colocalize with endosome markers. Immunocytochemistry of axons with (A) Rab11 and C-terminal APP Epitomics (APPE), (B) Rab5 and N-terminal A8967 (APPN), (C) Rab7 and C-terminal APP Jonas (APPJ), and (D) BACE and N-terminal APP 5a3/1g7 (APP5). Arrows indicate single-labeled APP vesicles. Arrowheads indicate double-labeled vesicles. Respective merged images are also shown. Scale bar: 5 µm. (E and F) Histogram plots of colocalization of two representative antibody pairs. Frequency of single-labeled puncta versus double-labeled puncta is plotted as a function of distribution along axon lengths.

Rab5 and Rab11 vesicle densities were unchanged, only Rab7 particles were diminished (p = 0.007; Figure 7C).The reduction of axonal C-terminal APP vesicles by only 10 ± 3% indicates that most of the axonal APP vesicles are still sorted into axons regardless of endocytic inhibition.

Next we calculated colocalization of APP, BACE, and endocytic markers in the human neurons. For antibody compatibility, one C- or N-terminal antibody was used with each vesicle marker. We found that, in the axons of human neurons, 48 ± 1.6% of APP-containing vesicles colocalized with BACE (Figure 7D), but colocalization did not change with dynasore treatment. This is higher than that reported in dendrites with exogenous labeled APP and BACE (Das *et al.*, 2013). Of all the vesicle types, the only significant change was a moderate decrease in the number of Rab11 particles colocalized with C-terminal APP (Figure 7E, from 42 ± 1.5% to 29 ± 0.73%, $p < 0.0001$, vehicle $n = 19$ axons, dynasore $n = 22$ axons). It is interesting that the only vesicle class affected was recycling endosomes, which have been shown to be necessary for APP processing. Also notable is the fact that ~75% of axonal APP vesicles in vehicle-treated conditions are positive for an endosomal marker.

Finally, the loading of protein into vesicles was measured by fluorescence intensity per puncta. In APP vesicles, several antibodies had statistically significant differences in staining intensity, but none were confirmed by a second antibody (Figure 7F). This may be due to the very large sample size and the flaws in specificity for each antibody (APP Jonas: 82 ± 2%, Mann-Whitney U-test $p < 0.001$, vehicle $n = 3238$ puncta, dynasore $n = 2467$ puncta; N-terminal A8967: 124 ± 3%, $p < 0.001$, vehicle $n = 2791$, dynasore $n = 2849$; N-terminal 5a3: 84±2%, $p < 0.001$, vehicle $n = 1908$, dynasore $n = 1685$).

A consistent change was observed in the amount of Rab11 and BACE loading in APP vesicles (Figure 7G). Rab11 levels increased in both C- and N-terminal–labeled APP vesicles (137 ± 6%, Mann-Whitney U-test: $p < 0.001$, vehicle $n = 398$ puncta, dynasore $n = 299$), while BACE levels were decreased in both C- and N-terminal–labeled APP vesicles (to 88 ± 2%, $p < 0.001$, vehicle $n = 349$, dynasore $n = 297$ and 85 ± 3%, $p < 0.001$, vehicle n vehicle $n = 381$, dynasore $n = 346$, respectively). Although the magnitude of the changes in loading on vesicles is not large, these population shifts are consistent with neuronal dependence on endocytosis for processed fragments, but most APP and BACE proteins enter the axon independent of endocytosis.

DISCUSSION

In this study, we have made three principal findings. First, we found that both mouse and human neurons secrete detectable amounts of APP fragments from axons and that axons contribute ~40% of the total secreted neuronal Aβ. Second, we demonstrated that a large fraction, ~80%, of the Aβ secreted from axons was processed in the cell soma in a secretase- and endocytosis-dependent pathway. Third, we identified multiple pathways for axonal sorting of APP, Aβ, and BACE, including both endosome-dependent and endosome-independent sorting. These pathways lead to packaging of most APP and its fragments into axonal vesicles that have endosomal markers, and a subpopulation that includes BACE, indicating that most axonal APP passes through an endosomal compartment before axonal entry and thus is primarily endosome derived. Together these findings indicate that the processing, sorting, and trafficking of APP and its fragments to axons are highly regulated in neurons and encompass multiple pathways.

Previous studies have focused on the role of APP processing in the pathology of AD. Much of this work, however, has been performed in nonneuronal cells or in neurons overexpressing APP. Biochemical and cellular evidence to date have implicated: 1) a major role for synaptic activity and endocytosis in Aβ

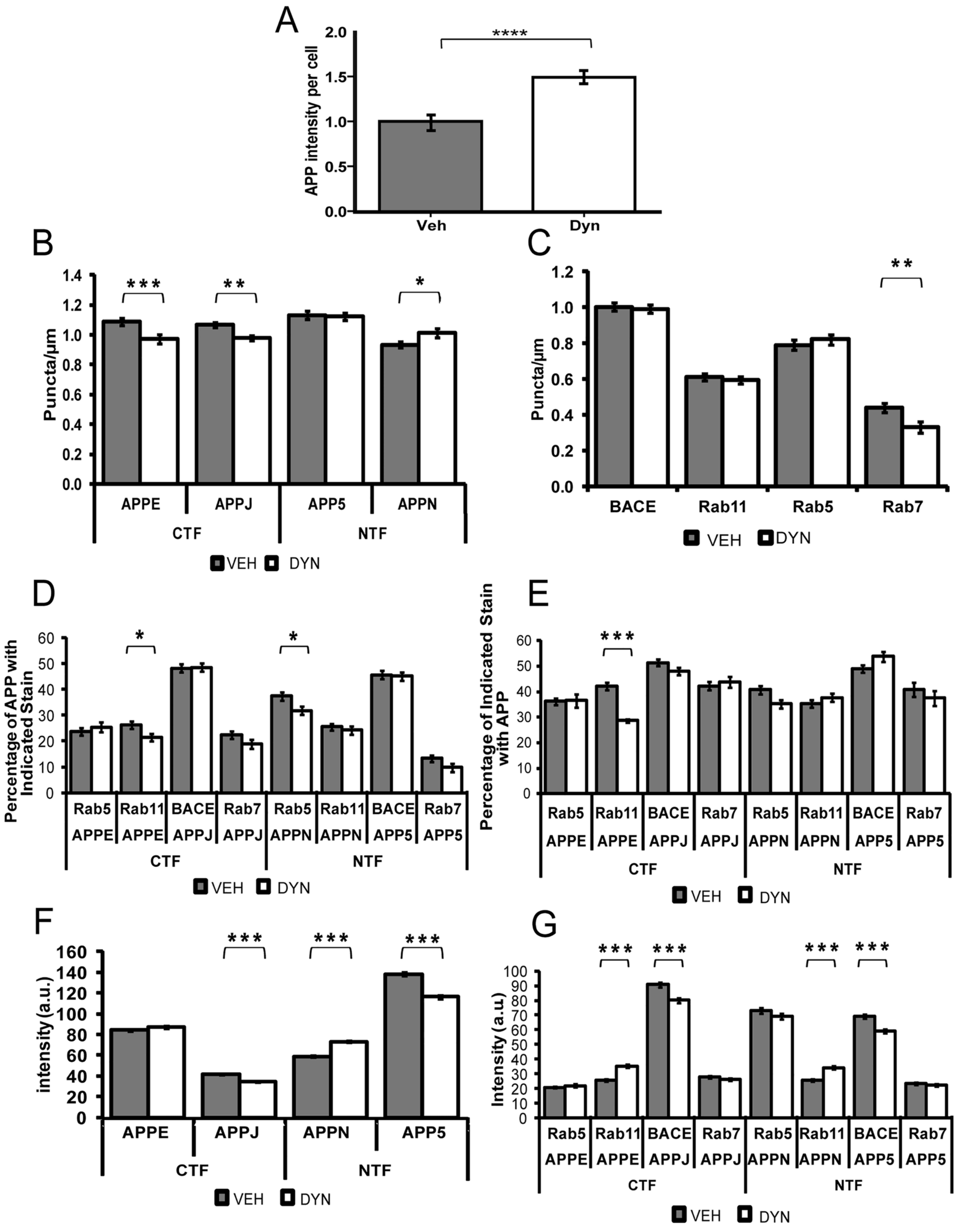

FIGURE 7: Axonal APP vesicle profiles are largely unchanged after endocytic inhibition. (A–G) Veh = DMSO; Dyn = dynasore. (A) Anti-APP antibody surface labeling intensity per cell, normalized to Whole Cell Blue labeling, in differentiated human neurons. Cells treated with DMSO or dynasore 18 h. (B) APP vesicle density per micrometer in human neurons after 18 h of endocytic inhibition. APPE = C-terminal Epitomics; APPJ = C-terminal Jonas; APP5 = N-terminal APP 5a3/1g7; APPN = N-terminal APP Sigma-Aldrich 8967. (C) Endosomal and BACE vesicle density. (D) Percentage of APP vesicles that colocalize with endosomal markers or BACE. (E) Percentage of endosome or BACE vesicles that also contain APP. (F) APP vesicle-staining intensity. (G) Endosomal marker or BACE intensity on APP vesicles. Error bars are SE; *, $p < 0.05$; **, $p < 0.01$; ***, $p < 0.001$.

production, 2) distal axons as one possible source of amyloid deposits, and 3) a link between axonal transport function and disease (Kamal *et al.*, 2000; Lazarov *et al.*, 2002; Abramov *et al.*, 2009; Das *et al.*, 2013).

Our studies of neurons using microfluidic chambers enabled us to directly measure the amounts of endogenous levels of secreted APP fragments without overexpression of any pathway components. By using this system, we discovered in mouse and human axons that

70–90% and 60–70%, respectively, of Aβ fragments were processed in the cell body before delivery to the axon. We also found that Aβ fragments, but not necessarily APP itself, depended upon endocytosis in the cell soma before being transported to axons. This requirement for "transcytosis" or some other endocytosis-dependent pathway before processing and fragment entry into axons represents a previously unknown requirement for APP fragment sorting and delivery into axons.

On the basis of our results, we can propose two models for APP sorting and processing that include a dependence on somatic endocytosis and processing. The first model is that APP itself goes to the axon through multiple distinct pathways. In this model, APP is sorted into axons via secretory vesicles, some of which merge before axonal entry with endosomes containing secretase complexes, and then APP and its fragments are sorted into axons in endosome-derived vesicles. Under this scenario, inhibition of endocytosis would prevent processing and would decrease the fragments bound for the axon, but direct-sorted APP would continue to arrive in the axon unprocessed, perhaps along with additional compensatory APP to maintain a consistent steady-state concentration. The sorting of APP into the axon despite endocytic inhibition is consistent with work in nonneuronal cells that found that C99–green fluorescent protein was sorted normally when dynamin is blocked (Kaether *et al.*, 2006).

A second model posits that APP and BACE are both endocytosed in the cell body, and at some point along the journey to the axon, the two vesicle types (clathrin dependent and independent) merge. In this case, perhaps APP and its processing machinery would continue to arrive in the axon while endocytosis is blocked, but without functional secretase activity, possibly due to disrupted timing or acidification. It is unlikely that altered BACE delivery into the axons alone causes the changes in axonal Aβ. This is supported by our finding that BACE levels in the axons decrease only slightly after endocytic inhibition and somatic inhibition of γ-secretase affects axonal Aβ, independent of β processing. These possibilities add an intriguing layer to the already complex regulation of APP processing and sorting in neurons.

Our finding that most axonally secreted Aβ comes from APP processed in the cell soma is surprising. Although one study theorized that APP must be processed in the cell soma before being sorted into axons, a majority of the prior evidence supports a model by which most APP is processed and secreted locally from axons (Kamal *et al.*, 2001; Cirrito *et al.*, 2008; Muresan *et al.*, 2009; Nikolaev *et al.*, 2009). It is important to note that these prior studies and our current results are not necessarily contradictory. One contributing factor to the apparent discrepancy is that these studies were performed in different neuronal types under different conditions. For example, it is plausible that neurons normally process most APP in the cell soma, but under stress, such as growth factor withdrawal, or in response to synaptic activity in mature synaptic circuits, local processing is activated (Nikolaev *et al.*, 2009; Das *et al.*, 2013). The axonal colocalization experiments in our current study show β-secretase present in axons, a majority of which is in the same vesicles as APP. An additional intriguing possibility is that localization of APP processing is in a dynamic equilibrium that responds to normal functions. Further investigation is needed to understand the circumstances regulating APP processing in axons versus soma and dendrites.

The complexity of APP processing engenders two interesting questions: 1) Is the location of processing in neurons shifted in response to damage or insult? 2) Do familial AD (FAD) mutations alter the location of processing and/or secretion? The first of these is of interest, because traumatic brain injury is a risk factor for AD, and previous work has focused on the damage responses of the brain contributing to disease (Van Den Heuvel *et al.*, 2007), which could be attributed to a neuronal stress response involving the location of processing or secretion. The second question stems from the observation that FAD mutations may also affect APP processing and sorting; previous work has shown that PS1 might normally regulate the exit of APP from the Golgi network, and FAD mutations in PS1 delay APP arrival at the cell surface. In addition to the early-onset familial mutations with a clear etiology, AD risk variants, such as those found in the *SorLA* or *ApoE* genes, are also connected to sorting of APP (Rogaeva *et al.*, 2007; Marzolo and Bu, 2009). SorLA influences the sorting of APP from late endosomes into recycling endosomes (Andersen *et al.*, 2005), suggesting that polymorphisms could change the subcellular sorting of APP and have subsequent downstream localization effects. These AD risk variants lend further credence to the importance of location of APP processing and Aβ secretion in AD. Our findings highlight the importance of determining whether risk variants affect the localization of processing, particularly in different neuronal compartments.

In summary, if the balance of somal versus axonal sorting and secretion is shifted in AD, it might be possible to screen for therapeutic agents that modulate this balance and shift the amyloid load away from axons and amyloid-sensitive synapses. Although there is still much to be learned about the pathological role of APP and Aβ, as well as other facets of AD, the development of more representative models, that include human neurons along with novel measurements of the cellular location of APP processing and Aβ secretion, represent important steps to overcoming this disease.

MATERIALS AND METHODS

cDNA constructs

Human APP- YFP in pcDNA3 was a gift from Christoph Kaether. mCherry pcDNA3 was a gift from Roger Tsien (University of California, San Diego).

Antibodies and cell lines

Primary antibodies and dilutions used: anti–N-terminal APP A8967 (1:100), GABA A2052 (1:1000), and human Map2a+b (1:1000) (Sigma-Aldrich, St. Louis, MO); N-terminal APP 5a3/1g7 (1:100) courtesy of Eddie Koo (Koo *et al.*, 1996); BACE 3D5 (1:200) courtesy of Robert Vassar (Zhao *et al.*, 2007); C-terminal APP Jonas clone (1:100), C-terminal APP AB5352 (1:100), NeuN (1:100), and Synaptophysin (1:100) (Chemicon/Millipore, Darmstadt, Germany); C-terminal APP Y188 (1:100) (Epitomics, Cambridge, UK); p-NFH SMI31 (1:2000) and βIIItub-Tuj1 rabbit and mouse monoclonal (1:2000) (Covance, Princeton, NJ); chicken anti-Map2 (1:1000) (Abcam, Cambridge, UK); Nestin (1:300) (Millipore, Billerica, MA); Rab5 (1:100) and Rab7 (1:100) (Santa Cruz, Dallas, TX); and Rab11 (1:100) (Becton Dickinson, Franklin Lakes, NJ). The cell lines used for differentiation of human neurons were PA6 stromal cells (Kawasaki *et al.*, 2000), and the hESC lines HUES9 (Harvard Stem Cell) and HSF6 (University of California, San Francisco). HUES9 were cultured on an irradiated mouse embryonic fibroblast (MEF) layer in HUES medium containing Knockout-DMEM (Life Technologies/Invitrogen, Carlsbad, CA), knockout serum replacement, nonessential amino acids, GlutaMAX, penicillin/streptomycin (pen/strep) and β-mercaptoethanol (Invitrogen), and 10 ng/ml bFGF (R&D Systems, Minneapolis, MN). HSF6 were grown on MEF feeder layers, in similar media, with the exception of Hi-glucose DMEM instead of Knockout-DMEM and without plasmanate.

Differentiation of hESCs into neurons

HUES9 or HSF6 ES cells were plated on 80% confluent PA6 feeder cells at a density of 125 cells/cm^2 in PA6 differentiation media composed of Glasgow DMEM, Knockout Serum Replacement (KSR), sodium pyruvate, GlutaMAX, pen/strep, and BME (all Invitrogen). For the first 6 d of culture, 500 ng/ml noggin (R&D Systems) and 10 μM SB431542 (Tocris, Bristol, UK) were added to PA6 differentiation media. After ~4 wk on PA6 cells, neural rosettes were hand selected and plated onto coverslips coated with poly-L-ornithine and laminin and cultured in Neuronal Media (ScienCell Research Labs, Carlsbad, CA) for 4–6 d. To induce neuronal differentiation, we transferred cultures into media containing DMEM:F12 + GlutaMAX, B27, N2, pen/strep (all from Invitrogen), 20 ng/ml BDNF, 20 ng/ml GDNF (Preprotech, Rocky Hill, NJ), and 0.5 mM db-cAMP (Sigma-Aldrich) for 4–5 wk. For imaging experiments, differentiated neurons were fluorescence-activated cell sorted for neurons, as described previously (Yuan *et al.*, 2011), and grown in glial-conditioned media. For immunocytochemistry of neuronal markers, cells on coverslips were fixed in 4% paraformaldehyde in phosphate-buffered saline (PBS) and blocked in 3% bovine serum albumin in PBS + 0.1% Triton-X-100. Primary antibodies were diluted in blocking buffer and incubated overnight. Alexa Fluor anti-rabbit, mouse (Invitrogen), and DyLight anti-chicken (Abcam) antibodies were incubated in blocking buffer for 1 h. Coverslips were mounted in ProLong Gold + 4′,6-diamidino-2-phenylindole (DAPI; Invitrogen).

Hippocampal neuron cultures

Hippocampal neurons were dissected from P0-P1 C57/BL6 or $APP^{+/-}$ or $APP^{-/-}$ ($App^{tm1Dbo/J}$) pups as previously described (Falzone *et al.*, 2009). Briefly, hippocampal brain sections were dissociated in papain and cultured in media containing Neurobasal-A, B27, and GlutaMAX on poly-L-lysine coated coverslips for 10 d before experimentation.

Compartmentalized microfluidic devices

Master molds were fabricated by photolithography, as previously described (Minteer, 2006), at the University of California, San Diego, Nano3 Cleanroom Facility. Devices were molded by soft lithography using Sylgard 182 (Ellsworth Adhesives, Germantown, WI) as previously described (Taylor *et al.*, 2005). Cured, cut devices were washed sequentially in isopropanol, water, and 70% ethanol, and then dried and mounted onto glass coverslips. For human neurons, compartments were plasma treated before mounting. Coverslips were coated with poly-L-lysine for hippocampal cultures or poly-L-ornithine/laminin for human neurons. For immunocytochemistry, neurons were fixed with 4% PFA + 4% sucrose, and subsequent staining steps were carried out within the chambers. For confirmation of fluidic isolation, 50 μg/ml 4-kDa FITC-dextran (Invitrogen) was added to cultures. Testing routinely was straightforward and relied on dextran introduction into both somal compartments, but not the axonal compartment, with the axonal compartment in isolation. After 24 h, samples from both somal and axonal compartments were collected and measured for dextran fluorescence.

Location of processing of APP and measurements of secretion

Neurons in compartments were transferred into fresh media, conditioned for 24 h, and then collected. A sample of original media was measured to account for the 10 μl of media retained in the axon compartment when the medium is changed. A protease inhibitor cocktail (Calbiochem/Millipore) was added, and the medium was kept at –80°C. Human Aβ40 and 42 were measured using a 6E10 electro-chemiluminescent immunoassay; mouse Aβ was measured using the 4G8 kit. Human sAPPβ, sAPPα, and MCP1 were also measured by electro-chemiluminescent immunoassay (MesoScale Discovery, Rockville, MD). For inhibitor experiments, 200 nM Compound E, 1 μM OM99-2, or 2 μM β-secretase inhibitor IV (all from EMD) was added to media for 24 h before collection. For normalization, compartments were fixed after media collection and labeled with βIIItub (mouse) or p-NFH (human) and DAPI. In the axonal chamber, the total number of βIIItub-positive projections were counted and used for normalization of secreted proteins. In the somal chamber, the average number of nuclei per frame were counted, and the average was used for normalization. In chambers containing human neurons, neuronal precursor cells occasionally can travel into the axonal compartment. When this occurred, these cells were counted, and their calculated contribution to axonal secreted proteins was subtracted, although their contribution was negligible.

Endocytosis dependence assays

Primary neurons were incubated with 100 μM dynasore (Tocris) for 24 h before fixation and immunocytochemistry for N- or C-terminal APP and Map2. For determining the efficacy of dynamin inhibition, 100 μg/ml Alexa Fluor 568–transferrin was added after drug treatment and incubated at 37°C for 30 min. For surface APP quantification, human neurons were incubated with vehicle or dynasore plus 22C11 antibody for 18 h. Cells were fixed but not permeabilized and then labeled with anti-mouse Alexa Fluor 488 as well as Whole Cell Blue Stain (Pierce/Thermo). Samples were imaged on a Zeiss 510 confocal microscope. For calculation of D:A ratio, Map2-positive or p-NFH–positive neurites were traced and measured using the NeuronJ plug-in for ImageJ (Meijering *et al.*, 2004).

APP-YFP live imaging

Hippocampal neurons on coverslips were cotransfected with APP-YFP and mCherry for 4 h using JetPrime (Polyplus-Transfection, Illkirch-Graffenstaden, France) and imaged 18 h after transfection. For dynasore drug treatment, medium containing 100 μM dynasore or dimethyl sulfoxide (DMSO) was added 4–6 h before imaging. Coverslips were imaged in a 37°C incubator with added CO_2. For ensuring axon identification in neurons treated with dynasore, axons were determined by morphology using mCherry fluorescence, and APP-YFP movement was imaged by stream acquisition at 100× magnification with 100-ms exposure for 15 s on a Nikon epifluorescence microscope with a CoolSnap camera. Cultures were maintained at 37°C and 5% CO_2 during imaging. Kymographs were analyzed in MetaMorph software.

Colocalization of endosome and APP markers

Hippocampal cultures were labeled by immunocytochemistry as described above and imaged on a Deltavision RT deconvolution microscope. Individual slices (without deconvolution) were processed for colocalization in Matlab using a package developed in our lab, described and extensively validated previously using a 300-nm cutoff for colocalization (Szpankowski *et al.*, 2012). For intensity measurements, the top and bottom 5% of vehicle-treated values were used as thresholds for all analyses.

Statistical analysis

Error bars in all charts represent SEM. Significance was calculated by one-way ANOVA followed by Tukey post hoc testing. Mouse Aβ values failed Levene's test for homoscedasticity and the Kolmogorov–Smirnov test for normality, so were log-transformed before ANOVA and back-transformed for reporting. For D:A ratios, significance was tested by ANCOVA (http://vassarstats.net/vsancova.html). Immunofluorescence measurements were tested by the nonparametric Mann-Whitney *U*-test. Calculations were performed with XL Toolbox version 6.52 by Daniel Kraus or GraphPad Prism.

REFERENCES

Abramov E, Dolev I, Fogel H, Ciccotosto GD, Ruff E, Slutsky I (2009). Amyloid-beta as a positive endogenous regulator of release probability at hippocampal synapses. Nat Neurosci 12, 1567–1576.

Andersen OM, Reiche J, Schmidt V, Gotthardt M, Spoelgen R, Behlke J, von Armin CA, Breiderhoff T, Jansen P, *et al.* (2005). Neuronal sorting protein-related receptor sorLA/LR11 regulates processing of the amyloid precursor protein. Proc Natl Acad Sci USA 102, 13461–13466.

Ascano M, Richmond A, Borden P, Kuruvilla R (2009). Axonal targeting of Trk receptors via transcytosis regulates sensitivity to neurotrophin responses. J Neurosci 29, 11674–11685.

Bel C, Oguievetskaia K, Pitaval C, Goutebroze L, Faivre-Sarrailh C (2009). Axonal targeting of Caspr2 in hippocampal neurons via selective somatodendritic endocytosis. J Cell Sci 122, 3403–3413.

Bertram L, Lill CM, Tanzi RE (2010). The genetics of Alzheimer disease: back to the future. Neuron 68, 270–281.

Brunholz S, Sisodia S, Lorenzo A, Deyts C, Kins S, Morfini G (2012). Axonal transport of APP and the spatial regulation of APP cleavage and function in neuronal cells. Exp Brain Res 217, 353–364.

Buytaert-Hoefen KA, Alvarez E, Freed CR (2004). Generation of tyrosine hydroxylase positive neurons from human embryonic stem cells after coculture with cellular substrates and exposure to GDNF. Stem Cells 22, 669–674.

Cai D, Leem JY, Greenfield JP, Wang P, Kim BS, Wang R, Lopes KO, Kim SH, Zheng H, Greengard P, *et al.* (2003). Presenilin-1 regulates intracellular trafficking and cell surface delivery of amyloid precursor protein. J Biol Chem 278, 3446–3454.

Carey RM, Balcz BA, Lopez-Coviella I, Slack BE (2005). Inhibition of dynamin-dependent endocytosis increases shedding of the amyloid precursor protein ectodomain and reduces generation of amyloid beta protein. BMC Cell Biol 6, 30–30.

Cataldo AM, Petanceska S, Peterhoff CM, Terio NB, Epstein CJ, Villar A, Carlson EJ, Staufenbiel M, Nixon RA (2003). App gene dosage modulates endosomal abnormalities of Alzheimer's disease in a segmental trisomy 16 mouse model of Down syndrome. J Neurosci 23, 6788–6792.

Chambers SM, Fasano CA, Papapetrou EP, Tomishima M, Sadelain M, Studer L (2009). Highly efficient neural conversion of human ES and iPS cells by dual inhibition of SMAD signaling. Nat Biotechnol 27, 275–280.

Cirrito JR, Kang JE, Lee J, Stewart FR, Verges DK, Silverio LM, Bu G, Mennerick S, Holtzman DM (2008). Endocytosis is required for synaptic activity-dependent release of amyloid-beta in vivo. Neuron 58, 42–51.

Coleman PD, Yao PJ (2003). Synaptic slaughter in Alzheimer's disease. Neurobiol Aging 24, 1023–1027.

Das U, Scott DA, Ganguly A, Koo EH, Tang Y, Roy S (2013). Activity-induced convergence of APP and BACE-1 in acidic microdomains via an endocytosis-dependent pathway. Neuron 79, 447–460.

Falzone TL, Stokin GB, Lillo C, Rodrigues EM, Westerman EL, Williams DS, Goldstein LSB (2009). Axonal stress kinase activation and tau misbehavior induced by kinesin-1 transport defects. J Neurosci 29, 5758–5767.

Garino C, Tomita T, Pietrancosta N, Laras Y, Rosas R, Herbette G, Maigret B, Quéléver G, Iwatsubo T, Kraus J-L (2006). Naphthyl and coumarinyl biarylpiperazine derivatives as highly potent human beta-secretase inhibitors. Design, synthesis, and enzymatic BACE-1 and cell assays. J Med Chem 49, 4275–4285.

Gunawardena S, Goldstein LSB (2001). Disruption of axonal transport and neuronal viability by amyloid precursor protein mutations in *Drosophila*. Neuron 32, 389–401.

Guo Q, Li H, Gaddam SSK, Justice NJ, Robertson CS, Zheng H (2012). Amyloid precursor protein revisited: neuron-specific expression and highly stable nature of soluble derivatives. J Biol Chem 287, 2437–2445.

Haass C, Kaether C, Thinakaran G, Sisodia S (2012). Trafficking and proteolytic processing of APP. Cold Spring Harb Perspect Med 2, a006270.

Israel MA, Yuan SH, Bardy C, Reyna SM, Mu Y, Herrera C, Hefferan MP, Van Gorp S, Nazor KL, Boscolo FS, *et al.* (2012). Probing sporadic and familial Alzheimer's disease using induced pluripotent stem cells. Nature 482, 216–220.

Kaether C, Schmitt S, Willem M, Haass C (2006). Amyloid precursor protein and Notch intracellular domains are generated after transport of their precursors to the cell surface. Traffic 7, 408–415.

Kamal A, Almenar-Queralt A, LeBlanc JF, Roberts EA, Goldstein LSB (2001). Kinesin-mediated axonal transport of a membrane compartment containing beta-secretase and presenilin-1 requires APP. Nature 414, 643–648.

Kamal A, Stokin GB, Yang Z, Xia C-H, Goldstein LSB (2000). Axonal transport of amyloid precursor protein is mediated by direct binding to the kinesin light chain subunit of kinesin-I. Neuron 28, 449–459.

Kawasaki H, Mizuseki K, Nishikawa S, Kaneko S, Kuwana Y, Nakanishi S, Nishikawa S-I, Sasai Y (2000). Induction of midbrain dopaminergic neurons from ES cells by stromal cell-derived inducing activity. Neuron 28, 31–40.

Kinoshita A, Fukumoto H, Shah T, Whelan CM, Irizarry MC, Hyman BT (2003). Demonstration by FRET of BACE interaction with the amyloid precursor protein at the cell surface and in early endosomes. J Cell Sci 116, 3339–3346.

Koo EH, Sisodia S, Archer DR, Martin LJ, Weidemann A, Beyreuther K, Fischer P, Masters CL, Price DL (1990). Precursor of amyloid protein in Alzheimer disease undergoes fast anterograde axonal transport. Proc Natl Acad Sci 87, 1561–1565.

Koo EH, Squazzo SL (1994). Evidence that production and release of amyloid beta-protein involves the endocytic pathway. J Biol Chem 269, 17386–17389.

Koo EH, Squazzo SL, Selkoe DJ, Koo CH (1996). Trafficking of cell-surface amyloid beta-protein precursor. I. Secretion, endocytosis and recycling as detected by labeled monoclonal antibody. J Cell Sci 109, 991–998.

Lai F, Williams RS (1989). A prospective study of Alzheimer disease in Down syndrome. Arch Neurol 46, 849–853.

Lazarov O, Lee M, Peterson DA, Sisodia SS (2002). Evidence that synaptically released beta-amyloid accumulates as extracellular deposits in the hippocampus of transgenic mice. J Neurosci 22, 9785–9793.

Leterrier C, Laine J, Darmon M, Boudin H, Rossier J, Lenkei Z (2006). Constitutive activation drives compartment-selective endocytosis and axonal targeting of type 1 cannabinoid receptors. J Neurosci 26, 3141–3153.

Lewczuk P, Esselmann H, Otto M, Maler JM, Henkel AW, Henkel MK, Eikenberg O, Antz C, Krause WR, Reulbach U, *et al.* (2004). Neurochemical diagnosis of Alzheimer's dementia by CSF $A\beta42$, $A\beta42/A\beta40$ ratio and total tau. Neurobiol Aging 25, 273–281.

Macia E, Ehrlich M, Massol R, Boucrot E, Brunner C, Kirchhausen T (2006). Dynasore, a cell-permeable inhibitor of dynamin. Dev Cell 10, 839–850.

Marzolo M-P, Bu G (2009). Lipoprotein receptors and cholesterol in APP trafficking and proteolytic processing, implications for Alzheimer's disease. Semin Cell Dev Biol 20, 191–200.

Meijering E, Jacob M, Sarria JC, Steiner P, Hirling H, Unser M (2004). Design and validation of a tool for neurite tracing and analysis in fluorescence microscopy images. Cytometry A 58, 167–176.

Minteer SD (2006). Microfluidic Techniques: Reviews and Protocols, Methods in Molecular Biology 321, New York: Springer.

Morel E, Chamoun Z, Lasiecka ZM, Chan RB, Williamson RL, Vetanovetz C, Dall'Armi C, Simoes S, Point Du Jour KS, McCabe BD, *et al.* (2013). Phosphatidylinositol-3-phosphate regulates sorting and processing of amyloid precursor protein through the endosomal system. Nat Commun 4, 2250.

Muresan Z, Muresan V (2007). The amyloid-beta precursor protein is phosphorylated via distinct pathways during differentiation, mitosis, stress, and degeneration. Mol Biol Cell 18, 3835–3844.

Muresan V, Varvel NH, Lamb BT, Muresan Z (2009). The cleavage products of amyloid-B precursor protein are sorted to distinct carrier vesicles that are independently transported within neurites. J Neurosci 29, 3565–3578.

Nikolaev A, McLaughlin T, O'Leary DDM, Tessier-Lavigne M (2009). APP binds DR6 to trigger axon pruning and neuron death via distinct caspases. Nature 457, 981–989.

Park JW, Kim HJ, Byun JH, Ryu HR, Jeon NL (2009). Novel microfluidic platform for culturing neurons: culturing and biochemical analysis of neuronal components. Biotechnol J 4, 1573–1577.

Rogaeva E, Meng Y, Lee JH, Gu Y, Kawarai T, Zou F, Katayama T, Baldwin C, Cheng R, Hasegawa H, *et al.* (2007). The neuronal sortilin-related receptor SORL1 is genetically associated with Alzheimer disease. Nat Genet 39, 168–177.

Sannerud R, Declerck I, Peric A, Raemaekers T, Menendez G, Zhou L, Veerle B, Coen K, Munck S, De Strooper B, *et al.* (2011). ADP ribosylation factor 6 (ARF6) controls amyloid precursor protein (APP) processing by mediating the endosomal sorting of BACE1. Proc Natl Acad Sci USA 108, E559–E568.

Schneider A, Rajendran L, Honsho M, Gralle M, Donnert G, Wouters F, Hell SW, Simons M (2008). Flotillin-dependent clustering of the amyloid precursor protein regulates its endocytosis and amyloidogenic processing in neurons. J Neurosci 28, 2874–2882.

Seiffert D, Bradley JD, Rominger CM, Rominger DH, Yang F, Meredith JE, Wang Q, Roach AH, Thompson LA, Spitz SM, *et al.* (2000). Presenilin-1 and -2 are molecular targets for g-secretase inhibitors. J Biol Chem 275, 34086–34091.

Simons M, Ikonen E, Tienari PJ, Cid-Arregui A, Monning U, Beyreuther K, Dotti CG (1995). Intracellular routing of human amyloid protein precursor: axonal delivery followed by transport to the dendrites. J Neurosci Res 41, 121–128.

Sleegers K, Brouwers N, Gijselinck I, Theuns J, Goossens D, Wauters J, Del-Favero J, Cruts M, Duijn CM van, Broeckhoven CV (2006). APP duplication is sufficient to cause early onset Alzheimer's dementia with cerebral amyloid angiopathy. Brain 129, 2977–2983.

Stachel SJ, Coburn CA, Steele TG, Jones KG, Loutzenhiser EF, Gregro AR, Rajapaske HA, Lai MT, Crouthamel MC, Xu M, *et al.* (2004). Structure-based design of potent and selective cell-permeable inhibitors of human beta-secretase (BACE-1). J Med Chem 47, 6447–6450.

Stokin GB, Lillo C, Falzone TL, Brusch RG, Rockenstein E, Mount SL, Raman R, Davies P, Masliah E, Williams DS, *et al.* (2005). Axonopathy and transport deficits early in the pathogenesis of Alzheimer's disease. Science 307, 1282–1288.

Szpankowski L, Encalada SE, Goldstein LSB (2012). Subpixel colocalization reveals amyloid precursor protein-dependent kinesin-1 and dynein association with axonal vesicles. Proc Natl Acad Sci USA 109, 8582–8587.

Tampellini D, Rahmen N, Gallo EF, Huang Z, Dumont M, Capetillo-Zarate E, Ma T, Zheng R, Lu B, Nanus DM, *et al.* (2009). Synaptic activity reduces intraneuronal Abeta, promotes APP transport to synapses, and protects against Abeta-related synaptic alterations. J Neurosci 29, 9704–9713.

Taylor AM, Blurton-Jones M, Rhee SW, Cribbs DH, Cotman CW, Jeon NL (2005). A microfluidic culture platform for CNS axonal injury, regeneration and transport. Nat Methods 2, 599–605.

Torroja L, Chu H, Kotovsky I, White K (1999). Neuronal overexpression of APPL, the *Drosophila* homologue of the amyloid precursor protein (APP), disrupts axonal transport. Curr Biol 9, 489–493.

Van Den Heuvel C, Thornton E, Vink R, John TW, Andrew IRM (2007). Traumatic brain injury and Alzheimer's disease: a review. Prog Brain Res 161, 303–316.

Wei W, Nguyen LN, Kessels HW, Hagiwara H, Sisodia S, Malinow R (2009). Amyloid beta from axons and dendrites reduces local spine number and plasticity. Nat Neurosci 13, 190–196.

Weisz OA, Rodriguez-Boulan E (2009). Apical trafficking in epithelial cells: signals, clusters and motors. J Cell Sci 122, 4253–4266.

Wisco D, Anderson ED, Chang MC, Norden C, Boiko T, Folsch H, Winckler B (2003). Uncovering multiple axonal targeting pathways in hippocampal neurons. J Cell Biol 162, 1317–1328.

Yamazaki T, Selkoe DJ, Koo EH (1995). Trafficking of cell surface beta-amyloid precursor protein: retrograde and transcytotic transport in cultured neurons. J Cell Biol 129, 431–442.

Yap CC, Wisco D, Kujala P, Lasiecka ZM, Cannon JT, Chang MC, Hirling H, Klumperman J, Winckler B (2008). The somatodendritic endosomal regulator NEEP21 facilitates axonal targeting of L1/NgCAM. J Cell Biol 180, 827–842.

Yuan SH, Martin J, Elia J, Flippin F, Paramban RI, Hefferan MP, Vidal JG, Mu Y, Killian RL, Israel M, *et al.* (2011). Cell-surface marker signatures for the isolation of neural stem cells, glia and neurons derived from human pluripotent stem cells. PLoS One 6, e17540.

Zhao J, Fu Y, Yasvoina M, Shao P, Hitt B, O'Connor T, Logan S, Maus E, Citron M, Berry R, *et al.* (2007). β-Site amyloid precursor protein cleaving enzyme 1 levels become elevated in neurons around amyloid plaques: implications for Alzheimer's disease pathogenesis. J Neurosci 27, 3639–3649.